

Impact of RE/Ba change on RE₂O₃ phase and BaZrO₃ nanorods at low temperature in REBCO superconducting film

Ziwei Zhou¹, Yanru Huang², Guojun Cai^{1*}, Raja Devesh Kumar Misra³

¹School of Mechanical Engineering, Liaoning Petrochemical University, Fushun 113001, P. R. China

²College of Science, Liaoning Petrochemical University, Fushun 113001, P. R. China

³Laboratory for Excellence in Advanced Steel Research, Department of Metallurgical, Materials and Biomedical Engineering, University of Texas at El Paso, El Paso, TX 79968, USA

Received 12 October 2024, received in revised form 8 November 2024, accepted 13 November 2024

Abstract

The critical current density (J_c) dependence on an applied magnetic field was studied for a prototype REBCO with Zr doping content coated conductor fabricated by metal-organic chemical vapor deposition (MOCVD). The study revealed that different rare-earth (RE) cations were incorporated into the superconducting film to form RE₂O₃ and BaZrO₃ (BZO). RE₂O₃ nanoparticles had a stronger pinning effect on magnetic flow along the direction of the a - b plane of films. With the increase of RE content, many RE₂O₃ nanoparticles effectively inhibited the precipitation of Ba-Cu-O heterophase, and when RE/Ba \geq 0.65, the increase of coarse Ba-Cu-O phases wrecked the continuity of matrix and crystal quality of films, causing a decrease on J_c (90°). After excessive RE elements (RE/Ba = 0.70) were doped in film, RE₂O₃ phases were changed from granular to lamellar and cut off the continuous growth of BZO along the c -axis, reducing J_c (0°) of films.

Key words: rare-earth barium copper oxide (REBCO), RE₂O₃, BZO, rare-earth (RE), critical current density (J_c)

1. Introduction

REBa₂Cu₃O_{7- δ} ((REBCO), RE = rare earth elements), which is called the second-generation high-temperature superconducting tape, has great potential applications in power transmission, energy storage, high energy physics, and military industry fields [1–3]. Compared with the first-generation high-temperature superconducting materials (bismuth series), REBCO has the obvious advantages of less anisotropy, higher irreversible magnetic field, and critical current density [4–6]. Electronic and structural anisotropy has been recognized as a vital source, accounting for this phenomenon: critical current density (J_c) values vary with the applied magnetic field. In an angular dependence measurement system, the a - b plane of lattice in a coated conductor is normally parallel to the film/substrate interface or film surface. The magnetic field angular dependence of J_c maximum, denoted as a - b peak, which is produced by a combined effect of layered defects, intrinsic pinning,

and electronic mass anisotropy, has been reported for REBCO films prepared by some techniques such as sputtering [7], metal-organic deposition (MOD) [8], pulsed laser deposition (PLD) [9], and metal-organic chemical vapor deposition (MOCVD) [10–12]. Among them, MOCVD is a very popular method in the field of nano-thin film preparation because of its capability for stoichiometric transfer from target to substrate surface and relatively high deposition rates (200–500 nm min⁻¹).

MacManus-Driscoll et al. [13] found that a type of heteroepitaxial addition BaZrO₃ (BZO) in REBCO superconducting film had a magnetic flux pinning ability, which was crucial for a greater enhancement in J_c . The structural and superconducting properties of MOCVD-derived REBCO films are sensitive to these parameters: deposition temperature, deposition rate, deposition pass, and film thickness. BZO nanoparticles parallel to the c -axis depend on correlated defects such as RE₂O₃ nanoparticles, and these deposition parameters are based on the experiments.

*Corresponding author: e-mail address: cgi197800@163.com

This paper aims to find a relationship between target density, coating characteristics, and related superconducting performance. To enhance the effect of flux pinning, Zr and RE (Y, Gd) were incorporated into multilayer superconducting films to form BZO and (Y,Gd)₂O₃ nanoparticles extended nearly parallel to the *c*-axis and *a*-*b* plane, respectively. The results of the present study optimize the manufacturing technique of superconducting films and provide a theoretical basis for improving the J_c of films.

2. Experimental procedure

2.1. Target preparation

REBCO films with Zr doping under study were deposited by MOCVD on an ion beam-assisted deposition (IBAD) MgO template that had a multilayer film structure of LaMnO₃/homoepitaxial-MgO/IBAD-MgO/Y₂O₃/Al₂O₃/Hastelloy C276 substrate. The details of film preparation were as follows: In brief, a precursor delivery system with precision metering pumps delivers Y, Gd, Ba, and Cu precursors at a constant flow rate. Then, the liquid precursor flashed in a constant temperature carburetor. The evaporated precursor was heated and injected into the hot substrate surface in the form of carrier gas (such as Ar) by the rectangular nozzle and then chemically reacted with oxygen to form REBCO film; after that, a protective Ag layer of 4 μm was deposited on the multilayer film by magnetron sputtering. Subsequently, they were annealed in flowing pure oxygen at 500 °C for 3.5 h so that the formed REBCO tetragonal phase could absorb oxygen fully and be transformed into a high-performance REBCO superconducting film.

2.2. Composition optimization of film

In this study, the Zr doping amount of films was 5 mol.%, the Cu/Ba value was 1.1, and the RE/Ba values were 0.55, 0.60, 0.65, and 0.70, respectively. The baseband of Hastelloy C276 alloy with a thickness of 65 μm, width of 12 mm, and multilayer oxide buffer structure was selected. All the film samples were prepared in the same production process, and the specific process parameters were as follows: the cavity pressure was 2.0 Torr, the partial oxygen pressure was 0.60 Torr, and the argon flow rate was 1.2 SLM. An inductively coupled atomic emission spectrometer (ICP-AES) was used to detect the chemical composition of samples, and the results are shown in Table 1.

With one pass of deposition, the deposition temperature was 870 °C, and the growth rate was 0.15 μm min⁻¹ for the superconducting layer, respectively. The Zr:REBCO film thicknesses were all about 0.9 μm, measured by transmission electron microscopy

Table 1. Chemical composition test results of REBCO films with different RE/Ba (wt.%)

RE/Ba	Zr:Gd:Y:Ba:Cu (In the chemical source)	Zr:Gd:Y:Ba:Cu (In the film)
0.55	0.05:0.55:0.55:2.00:2.20	0.04:0.58:0.58:2.00:2.20
0.60	0.05:0.60:0.60:2.00:2.20	0.04:0.61:0.61:2.00:2.20
0.65	0.05:0.65:0.65:2.00:2.20	0.04:0.66:0.66:2.00:2.21
0.70	0.05:0.70:0.70:2.00:2.20	0.04:0.71:0.71:2.00:2.20

(TEM). The film sample was bonded to the silicon wafer with the prepared glue. After the bonding, the sample was fixed with a fixture and then placed on a heating table for curing treatment. The heating temperature was 140 °C, and the holding time was 1.5 h. The bonded sample was fixed with paraffin wax before grinding it with sandpaper. When the sample thickness was reduced to half of the original thickness, turn over and continue grinding until the thickness was about 50 μm. The operating temperature of the ion thinning instrument was thinned and set at -150 °C, and the energy was 5 keV by the ion thinning meter. It was important to note that the arrays of aligned BZO and (Y,Gd)₂O₃ nanoparticles formed in the directions nearly parallel to the *c*-axis and the *a*-*b* plane, respectively.

2.3. Liquid nitrogen temperature critical current test

REBCO films with Zr doping were measured at liquid nitrogen temperature using the four-probe method. The main measurement steps were as follows: two groups of wires were drawn on the surface of film samples, one group of wires was connected to the program-controlled DC current source, and the other was connected to the acceptor voltmeter. Because of high critical current values observed at lower temperatures, 50 μm × 50 μm samples were cut by Nd:YAG (yttrium aluminum garnet) laser for J_c measurement at 77 K in fields up to 3 T to avoid harmful Joule heating and overstressing. Meanwhile, the critical current measurement system was tested in the -180 °C–180 °C range, and the samples were immersed in liquid nitrogen to make them superconducting. Then, an increasing current was introduced using a DC current source under the control of a set program when 1 μV cm⁻¹ on another set of wires was used as the blackout criterion of the film by a nanovoltmeter.

3. Results and discussion

3.1. Structure properties of film

The microstructures and typical buffer layer of

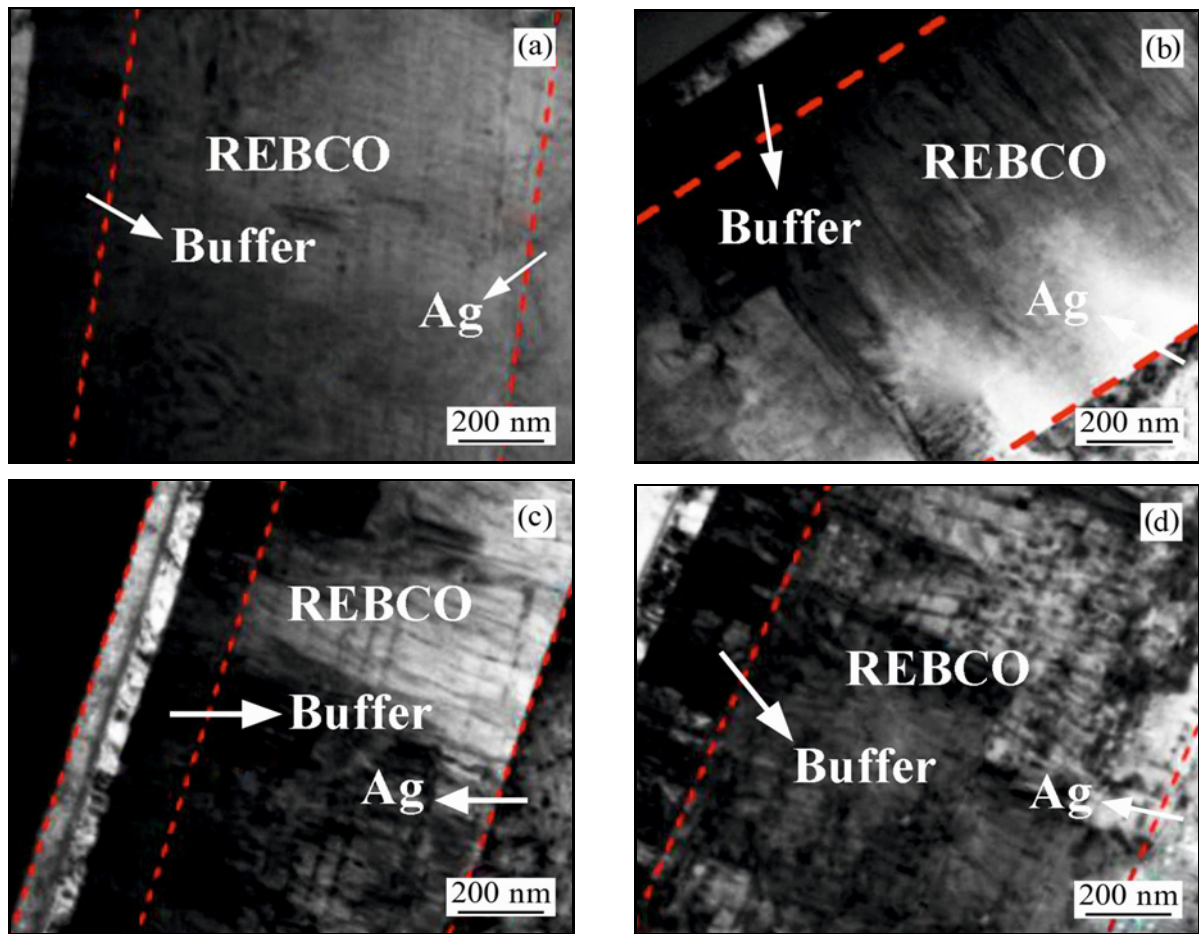


Fig. 1. TEM section microstructures and typical buffer layer of films: (a) RE/Ba = 0.55, (b) RE/Ba = 0.60, (c) RE/Ba = 0.65, and (d) RE/Ba = 0.70.

films are observed by TEM, as shown in Fig. 1. It is observed from the figures that these films are composed of Hastelloy layer (baseband layer), buffer layer, Zr:REBCO film layer, and metal Ag protective layer. Many columnar structures are formed in films in the thickness direction of the Zr:REBCO layer. Combined with TEM observation results on the surface, it can be determined that these columnar structures are mainly self-assembled BZO nanocolumns, as shown in Figs. 1a–c. It can be observed from Fig. 1d that RE_2O_3 lamellae cut the BZO growing along the c -axis into two sections, which indicates that excessive RE elements (RE/Ba = 0.70) destroy the continuous growth of BZO nanocolumns and shorten their effective length.

The comparison of cross-sectional-view TEM microstructures and the corresponding length statistics of BZO nanocolumns are shown in Fig. 2. For Zr:REBCO films, a large number of slender and smaller BZO nanocolumns which only nucleate on the surface of the film, are uniformly distributed along c -axis (Figs. 2a,b). With the gradual increase in RE/Ba content, the deposited atoms have enough en-

ergy to move to the region with low mismatch and continue to grow, making the length of BZO larger, and the length of BZO nanocolumns gradually increases, and the arrangement is orderly (Figs. 2c,d). When RE/Ba content is up to 0.70, a large amount of lamellar RE_2O_3 truncates the BZO along the c -axis, affecting their continuous growth and weakening the pinning effect of BZO nanocolumns.

3.2. Surface morphology of Zr:REBCO film

Figure 3 presents SEM surface morphologies of films with different RE/Ba. As can be seen from the figure, Zr:REBCO films as a whole have mainly two-dimensional lamellar growth patterns, accompanied by local three-dimensional islands of Ba-Cu-O phases. A large number of coarse Ba-Cu-O phases ($\sim 0.5 \mu\text{m}$) can be observed on the film's surface (Fig. 3a), resulting in the poor crystallization quality of the film. When RE/Ba = 0.60, the precipitate amount of Ba-Cu-O phases is significantly reduced because the formation of RE_2O_3 nanoparticles effectively inhibits the precipitate of Ba-Cu-O impurity phase (Fig. 3b). The

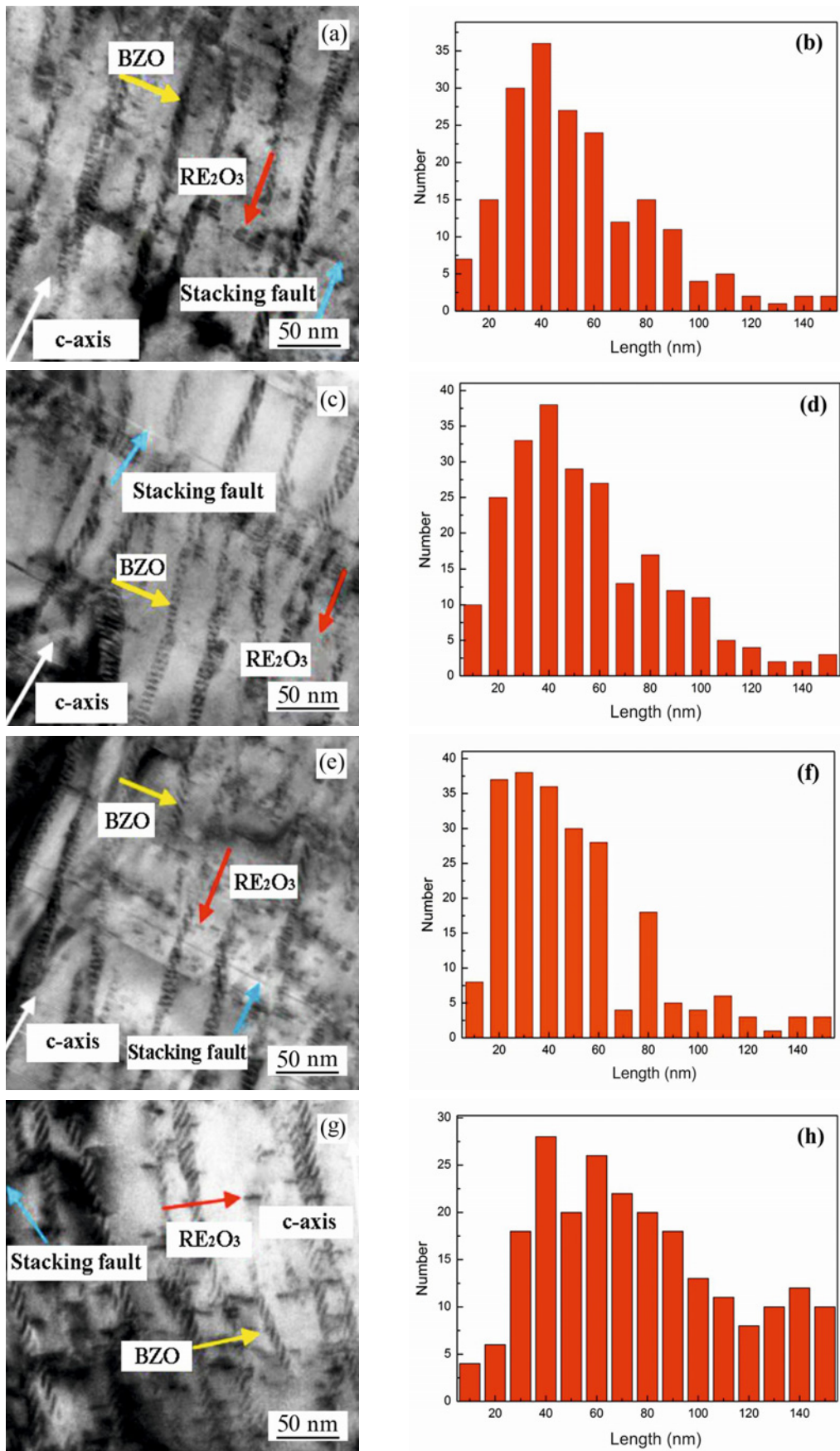


Fig. 2. Comparison of cross-sectional-view TEM microstructures and the corresponding length statistics of BZO nanocolumns of films: (a), (b) RE/Ba = 0.55; (c), (d) RE/Ba = 0.60; (e), (f) RE/Ba = 0.65; and (g), (h) RE/Ba = 0.70.

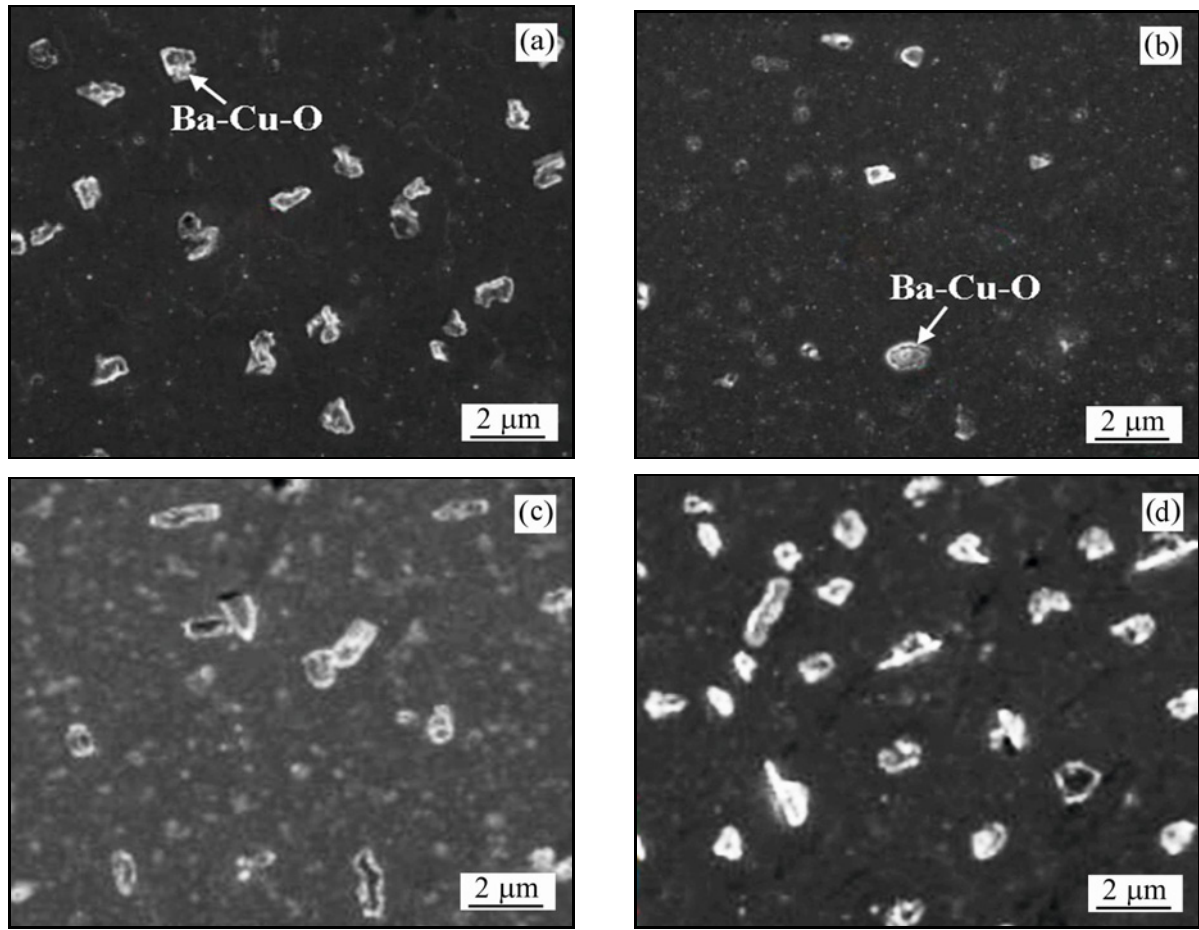


Fig. 3. SEM surface morphologies of films with different RE/Ba: (a) RE/Ba = 0.55, (b) RE/Ba = 0.60, (c) RE/Ba = 0.65, and (d) RE/Ba = 0.70.

precipitation amount of coarse Ba-Cu-O phases increases with increasing of RE/Ba (Figs. 3c,d), which may be the result of the increasing size of RE₂O₃ nanoparticles, and they cannot inhibit the precipitation of Ba-Cu-O phases.

Figure 4 shows the TEM surface morphologies of films with different RE/Ba. It is found that with the increase of RE content, the diameter of BZO nanocolumns does not change significantly, and their distribution is uniform, which indicates that the change of RE element content has little influence on the diameter and distribution of BZO. However, the number of BZO, which becomes the effective pinning center, decreases significantly when RE/Ba = 0.70 (Fig. 4d).

Deposited atoms are more likely to nucleate and grow at sites with less lattice mismatch. Therefore, when the BZO phases nucleate in the matrix during the deposition of films, it can continue to grow at the nucleated point in a self-composed manner, and its growth direction is mainly related to the mismatch degree (f).

$$f = \frac{a - a'}{a'} \times 100\%, \quad (1)$$

where a represents the lattice constant of the BZO phase, and a' is the lattice constant of the Zr:REBCO matrix. The larger lattice constants of BZO and matrix in the c -axis direction of the film affect their lattice mismatch because part of Ba atoms occupies the positions of RE atoms in the film, and the radius of Ba atoms is larger than that of RE atoms [14–17].

Figure 5 shows the formation mechanism of pinning defects in Zr:REBCO film samples with different RE/Ba. When RE/Ba = 0.55, some BZO nanocolumns, RE₂O₃ particles and coarse Ba-Cu-O phases occur in the film (Fig. 5a), and the precipitation of Ba-Cu-O phases can be effectively inhibited by the increasing of granular RE₂O₃ particles in the film (Fig. 5b). When RE/Ba increases to 0.65, RE₂O₃ phases gradually change from granular to lamellar, but they do not affect the continuous growth of BZO. In this case, RE₂O₃ nanoparticles and BZO are distributed along the a - b plane and c -axis of the film to form a two-dimensional pin array, as shown in Fig. 5c. When RE/Ba = 0.70, BZO nanocolumns grow along c -axis into two sections, cut by RE₂O₃ lamellae, and more RE elements can destroy the continuous growth of BZO and shorten their effective length (Fig. 5d).

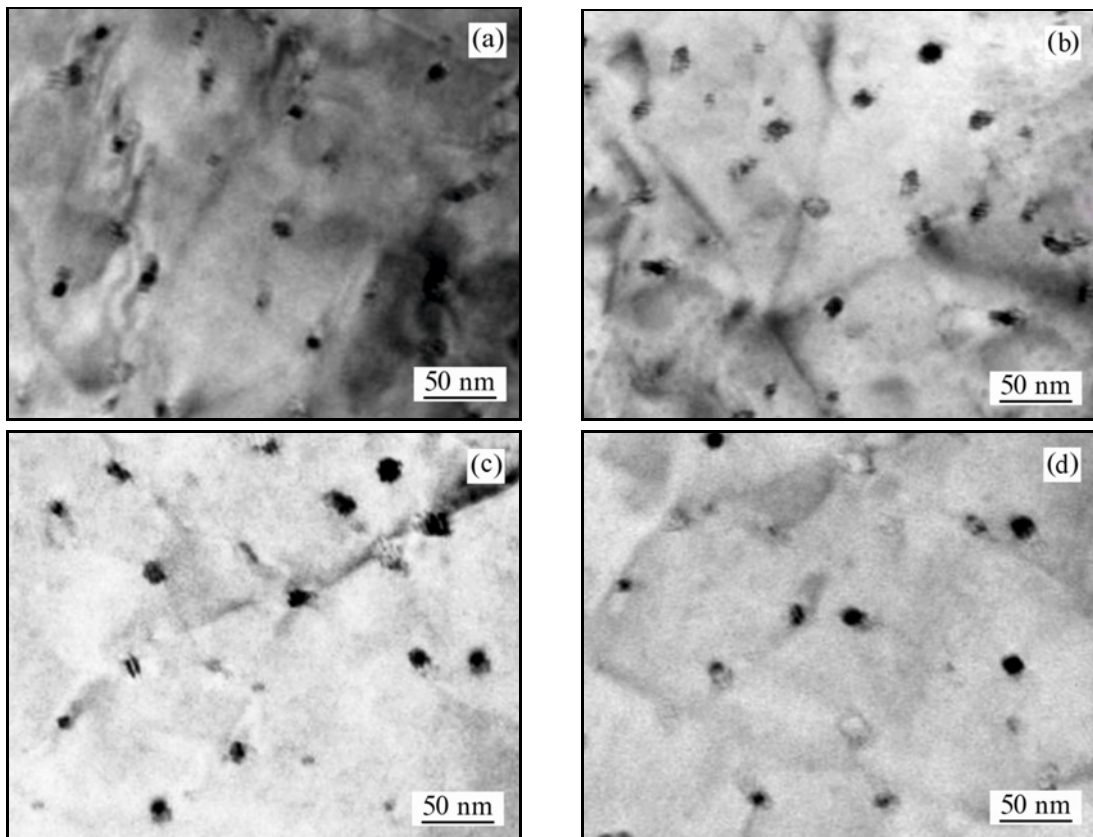


Fig. 4. TEM surface morphologies of films with different RE/Ba: (a) RE/Ba = 0.55, (b) RE/Ba = 0.60, (c) RE/Ba = 0.65, (d) RE/Ba = 0.70.

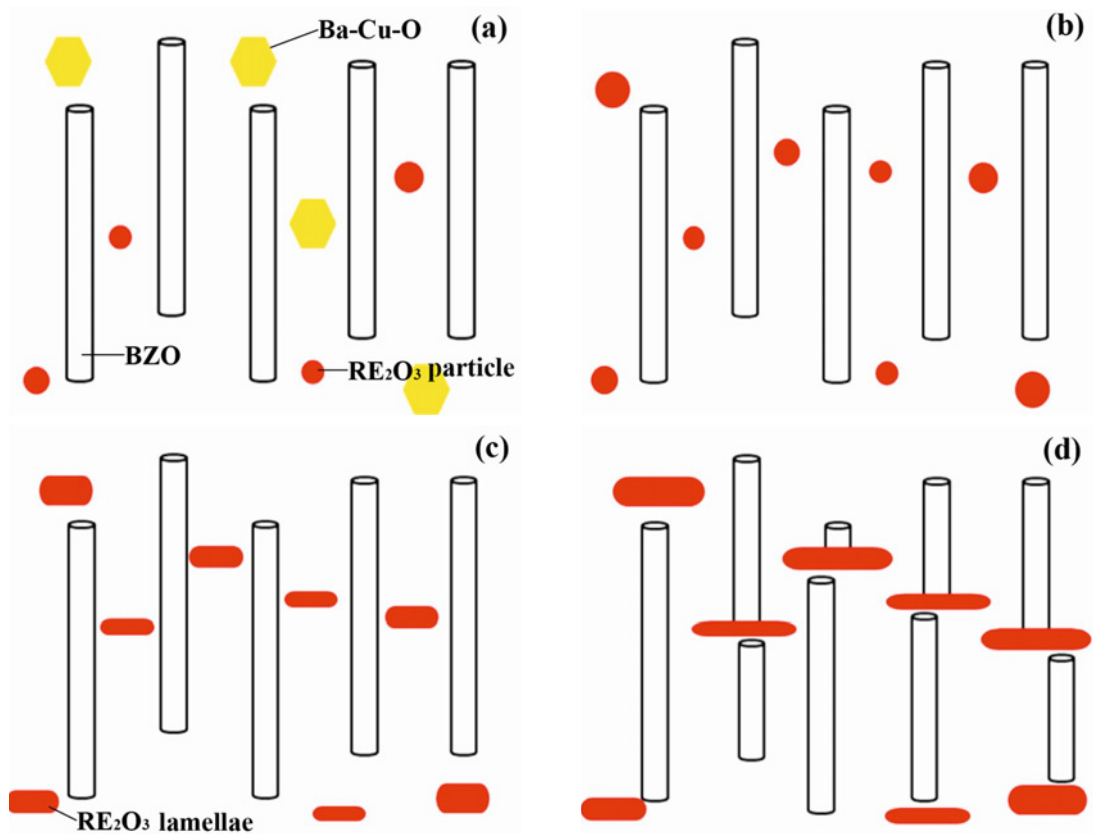


Fig. 5. Influence of RE/Ba on the formation mechanism of pinning defects in Zr:REBCO film: (a) RE/Ba = 0.55, (b) RE/Ba = 0.60, (c) RE/Ba = 0.65, and (d) RE/Ba = 0.70.

The inherent layered structure and anisotropy of Zr:REBCO superconducting material made the a - b plane larger and the c -axis smaller, which were also presented by Kwak et al. [18]. To obtain high J_c , the out-of-plane grains are oriented along the c -axis, and the in-plane grains are neatly arranged along the a -axis and b -axis, thus forming excellent biaxial textures [19, 20]. For this reason, RE_2O_3 particles in Zr:REBCO film aligned along the a - b plane are proved to have an effective three-dimensional pinning defect only when the direction of the applied magnetic field is parallel to the a - b plane of the Zr:REBCO film and this film has a large J_c . However, due to its strong anisotropy, once the direction of the applied magnetic field deviates from the a - b plane, J_c decreases rapidly. Therefore, the only way to obtain the excellent current-carrying capacity of films is to effectively reduce the influence of anisotropy without reducing the direction conductivity of the a - b plane.

3.3. Superconducting performance of Zr:REBCO film

Figure 6 reveals the change of J_c (77 K, 0 T) with RE/Ba. After the applied magnetic field is carried out on the B// a - b plane (i.e., the angle is 90°) and the B// C axis (i.e., the angle is 0°), J_c varies with RE/Ba. Since pinning by correlated disorder always reduces the system energy, vortex lines incline to align themselves parallel to extended defects that act as effective pinning centers, such as those granular or lamellar RE_2O_3 nanoparticles occur in a - b plane while columnar BZO form along c -axis. Depending on the applied magnetic field, one factor can be dominant while another or others may be small.

When the direction of the applied magnetic field is parallel to the a - b plane, the coarse Ba-Cu-O makes the crystal quality of the film poor, resulting in a smaller J_c (90°). With the increase of RE content, a large number of RE_2O_3 nanoparticles effectively inhibit the precipitation of Ba-Cu-O heterophase, which causes a significant increase of J_c (90°). When $\text{RE}/\text{Ba} \geq 0.65$, the amount of coarse Ba-Cu-O phases increases significantly, and a possible explanation is that the increasing size of RE_2O_3 nanoparticles makes it difficult to play a strong magnetic flux pin in the a - b plane of film. Meanwhile, coarse Ba-Cu-O phases wreck the continuity of the matrix and crystal quality of films, causing a decrease in J_c (90°). It should be emphasized here that the higher J_c (0°) is attributed to the stronger magnetic flux pinning ability generated in the c -axis direction of the film ($\text{RE}/\text{Ba} = 0.65$) because of the continuous growth of BZO nanocolumns. After excessive RE elements ($\text{RE}/\text{Ba} = 0.70$) are doped in the film, RE_2O_3 phases are changed from granular to lamellar, and the continuous growth of

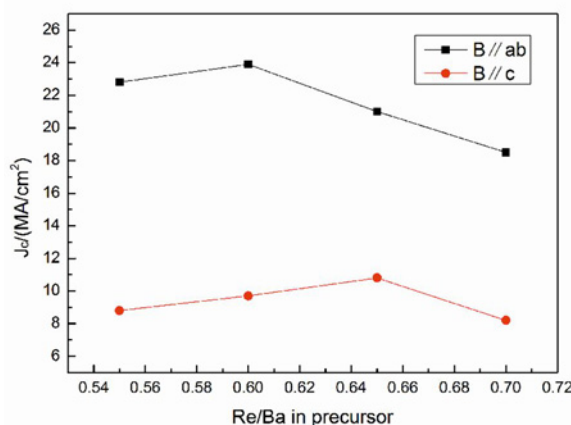


Fig. 6. J_c (77 K, 0 T) changed with RE/Ba.

BZO is cut along the c -axis, reducing the J_c (0°) value.

4. Conclusions

This work studied the prototype REBCO with Zr doping content coated conductor fabricated by metal-organic chemical vapor deposition (MOCVD) on buffered flexible metal Hastelloy C276 substrates. The main conclusions are as follows:

1. The Zr:REBCO films are deposited on buffered flexible metal Hastelloy C276 substrates by metal-organic chemical vapor deposition (MOCVD), adding RE/Ba varied from 0.55 to 0.70. RE_2O_3 nanoparticles in films mainly grow along the direction of the a - b plane, so their pinning effect on magnetic flow is stronger in the direction of the a - b plane of films.
2. With the increase of RE content, many RE_2O_3 nanoparticles effectively inhibit the precipitation of Ba-Cu-O heterophase and cause a significant increase of J_c (90°). When $\text{RE}/\text{Ba} \geq 0.65$, the increase of coarse Ba-Cu-O phases wrecks the continuity of matrix and crystal quality of films, causing a decrease in J_c (90°). The stronger magnetic flux pinning ability generated in the c -axis direction of the film ($\text{RE}/\text{Ba} = 0.65$) is due to the continuous growth of BZO nanocolumns.
3. After excessive RE elements ($\text{RE}/\text{Ba} = 0.70$) are doped in film, RE_2O_3 phases changed from granular to lamellar, affecting their pinning effect and cutting off continuous growth of BZO along the c -axis, reducing J_c (0°) of films.

Acknowledgements

This study was supported by the Foundation of the Department of Education of Liaoning Province (Grant

No. JYTMS20231429 and Grant No. LJKMZ20220727) and the College Students' Innovative Entrepreneurial Training Plan Program of Liaoning Province (Grant No. X202410148056).

References

- [1] L. H. Jin, C. S. Li, Z. M. Yu, J. Q. Feng, S. N. Zhang, A. Sulpice, Y. Wang, P. X. Zhang, Wrinkling of $\text{YBa}_2\text{Cu}_3\text{O}_{7-x}$ film prepared by trifluoroacetate metal-organic deposition, *Appl. Surf. Sci.* 355 (2015) 736–742.
<https://doi.org/10.1016/j.apsusc.2015.07.093>
- [2] S. Mukoyama, M. Yagi, N. Hirano, N. Amemiya, N. Kashima, S. Nagaya, T. Izumi, Y. Shiohara, Study of a YBCO HTS transmission cable system, *Physica C* 463–465 (2007) 1150–1153.
<https://doi.org/10.1016/j.physc.2007.03.452>
- [3] Y. Zhang, E. D. Specht, C. Cantoni, D. K. Christen, J. R. Thompson, J. W. Sinclair, A. Goyal, Y. L. Zuev, T. Aytug, M. P. Paranthaman, Y. Chen, V. Selvamannickam, Magnetic field orientation dependence of flux pinning in (Gd,Y) $\text{Ba}_2\text{Cu}_3\text{O}_{7-x}$ coated conductor with tilted lattice and nanostructures, *Physica C* 469 (2009) 2044–2051.
<https://doi.org/10.1016/j.physc.2009.08.007>
- [4] L. F. Liu, Y. J. Li, X. Wu, Y. J. Yao, M. L. Wang, B. B. Wang, Effect of target density on the growth and properties of YGBCO thin films deposited by pulsed laser deposition, *Appl. Surf. Sci.* 388 (2016) 77–81.
<https://doi.org/10.1016/j.apsusc.2016.03.151>
- [5] A. Mitani, R. Teranishi, K. Yamada, N. Mori, M. Mukaida, T. Kiss, M. Inoue, Y. Shiohara, T. Izumi, K. Nakaoka, J. Matsuda, Effect of fabrication conditions on crystalline of SmBCO films fabricated by TFA-MOD method, *Physica C* 468 (2008) 1546–1549.
<https://doi.org/10.1016/j.physc.2008.05.066>
- [6] T. Manabe, M. Sohma, I. Yamaguchi, K. Tsukada, W. Kondo, K. Kamiya, T. Tsuchiya, S. Mizuta, T. Kumagai, Surface resistances of 5-cm-diameter YBCO films prepared by MOD for microwave applications, *Physica C* 445–448 (2006) 823–827.
<https://doi.org/10.1016/j.physc.2006.04.042>
- [7] Y. Xue, Y. H. Zhang, F. Zhang, R. P. Zhao, H. Wang, J. Xiong, B. W. Tao, Growth of simplified buffer template on flexible metallic substrates for $\text{YBa}_2\text{Cu}_3\text{O}_{7-\delta}$ coated conductors, *J. Alloy Compd.* 673 (2016) 47–53.
<https://doi.org/10.1016/j.jallcom.2016.02.175>
- [8] H. Hochmuth, M. Lorenz, Side-selective and non-destructive determination of the critical current density of double-sided superconducting thin films, *Physica C* 265 (1996) 335–340.
[https://doi.org/10.1016/0921-4534\(96\)00303-6](https://doi.org/10.1016/0921-4534(96)00303-6)
- [9] T. Wang, S. Zhang, M. J. Yang, R. Tu, T. Goto, L. M. Zhang, Effect of precursors' ratio on c-axis-oriented SmBCO film by MOCVD, *Ceram. Int.* 43 (2017) S488–S492.
<https://doi.org/10.1016/j.ceramint.2017.05.219>
- [10] K. Matsumoto, T. Horide, K. Osamura, M. Mukaida, Y. Yoshida, A. Ichinose, S. Horii, Enhancement of critical current density of YBCO films by the introduction of artificial pinning centers due to the distributed nano-scaled Y_2O_3 islands on substrates, *Physica C* 412 (2004) 1267–1271.
<https://doi.org/10.1016/j.physc.2004.01.157>
- [11] A. Abrutis, A. Bartasyte, Z. Saltyte, A. Zukova, S. Donet, F. Weiss, Thick SmBCO layers and SmBCO/YBCO structures grown by pulsed injection MOCVD, *Physica C* 415 (2004) 21–28.
<https://doi.org/10.1016/j.physc.2004.07.016>
- [12] H. S. Ha, H. S. Kim, J. S. Yang, Y. H. Jung, R. K. Ko, K. J. Song, D. W. Ha, S. S. Oh, H. K. Kim, K. K. Yoo, S. I. Yoo, C. Park, D. J. Youm, S. H. Moon, J. H. Joo, Critical current density of SmBCO coated conductor on IBAD-MgO substrate fabricated by co-evaporation, *Physica C* 463–465 (2007) 493–496.
<https://doi.org/10.1016/j.physc.2007.01.039>
- [13] F. Fan, Y. M. Lu, L. L. Ying, Z. Y. Liu, C. B. Cai, R. Hühne, B. Holzapfel, Epitaxial growth of $\text{Ce}_2\text{Y}_2\text{O}_7$ buffer layers for $\text{YBa}_2\text{Cu}_3\text{O}_{7-\delta}$ coated conductors using reel-to-reel DC reactive sputtering, *Physica C* 471 (2011) 471–475.
<https://doi.org/10.1016/j.physc.2011.04.010>
- [14] Y. J. Yao, L. F. Liu, X. Wu, B. B. Wang, S. D. Lu, W. Wang, Y. J. Li, In-field superconducting critical current of $\text{Y}_{0.5}\text{Gd}_{0.5}\text{Ba}_2\text{Cu}_3\text{O}_{7-\sigma}$ films obtained by a multi-step deposition process, *Ceram. Int.* 43 (2017) 13524–13529.
<https://doi.org/10.1016/j.ceramint.2017.07.058>
- [15] T. S. Krylova, I. A. Chernykh, M. Y. Chernykh, E. P. Krasnoperov, M. L. Zhanavskina, $\text{YBa}_2\text{Cu}_3\text{O}_x$ - SrTiO_3 multilayer approach on textured Ni-W tapes: morphology, structure and critical current density improvement, *Thin Solid Films* 598 (2016) 289–292.
<https://doi.org/10.1016/j.tsf.2015.12.030>
- [16] Y. Xue, Y. H. Zhang, F. Zhang, R. P. Zhao, H. Wang, J. Xiong, B. W. Tao, Growth of simplified buffer template on flexible metallic substrates for $\text{YBa}_2\text{Cu}_3\text{O}_{7-\delta}$ coated conductors, *J. Alloy Compd.* 673 (2016) 47–53.
<https://doi.org/10.1016/j.jallcom.2016.02.175>
- [17] G. N. Xiao, L. F. Liu, D. Xu, X. Wu, Q. Luo, Y. J. Li, Influence of assisting ion beam current on the microstructure and surface morphology of IBAD-MgO thin films for YBCO coated conductors, *Surf. Coat. Technol.* 252 (2014) 108–112.
<https://doi.org/10.1016/j.surfcoat.2014.04.052>
- [18] K. Kwak, J. Rhee, W. Lee, H. Lee, D. Youm, J. Yoo, Effects of vortex line shape on critical current density in high T_c superconducting film with nanorod pinning centers under applied magnetic field of various orientations, *Physica C* 486 (2013) 51–57.
<https://doi.org/10.1016/j.physc.2013.01.003>
- [19] G. Kim, H. J. Jin, W. Jo, D. H. Nam, H. Cheong, H. S. Kim, S. S. Oh, R. K. Ko, Y. S. Jo, D. W. Ha, Ultra-large current transport in thick $\text{SmBa}_2\text{Cu}_3\text{O}_{7-x}$ films grown by reactive Co-evaporation, *Physica C* 513 (2015) 29–34.
<https://doi.org/10.1016/j.physc.2015.03.019>
- [20] H. Suzuki, Y. Yoshida, Y. Ichino, Y. Takai, S. Awaji, K. Watanabe, M. Yoshizumi, T. Izumi, Y. Shiohara, T. Kato, J_c anisotropy for magnetic field angle in YBCO coated conductor on IBAD-MgO buffered metal tapes, *Physica C* 470 (2010) 1384–1387.
<https://doi.org/10.1016/j.physc.2010.05.119>